Supporting Information

Evaluation of hybrid amine and alcohol solvent with ion-exchange resin catalysts for energy-efficient CO_2 capture

Qiang Sun[a], Jia Xiong[a], Hongxia Gao[a, *], Teerawat Sema[b], Wilfred Olson[a], Zhiwu Liang[a, *]

[a]Joint International Center for CO_2 Capture and Storage (iCCS), Provincial Hunan Key Laboratory for Cost-effective Utilization of Fossil Fuel Aimed at Reducing CO_2 Emissions, College of Chemistry and Chemical Engineering, Hunan University, Changsha, 410082, PR China

[b]Department of Chemical Technology, Faculty of Science, Chulalongkorn University, Bangkok, 10330, Thailand

* Author for correspondence:

Email: hxgao@hnu.edu.cn (Dr. H Gao), zwliang@hnu.edu.cn (Dr. Z Liang)

The supporting information contains 15 pages, and 7 Figures.

Content

Captions of Figure and Table

Figure S1. Schematic diagram of the experimental apparatus for CO_2 desorption and absorption.

Figure S2. The CO_2 desorption rate curves with different catalysts at 80 °C.

Figure S3. The CO_2 desorption performance with different initial CO_2 loading. (a) CO_2 desorption rate curves. (b) Total amount of CO_2 desorbed at 1200 s.

Figure S4. Raman spectra of MEA solution at various periods. (a) CO_2 desorption without catalyst. (b) CO_2 desorption with 2 wt.% Amberlyst-15.

Figure S5. The CO_2 desorption performance with different catalyst/MEA solvent ratios. (a) CO_2 desorption rate curves. (b) Total amount of CO_2 desorbed and relative heat duty at 1200 s.

Figure S6. Effect of methanol concentration on CO_2 desorption performance at 90 °C. (a) CO_2 desorption rate curves. (b) CO_2 loading curves. (c) Desorbed CO_2 amount curves. (d) Total amount of CO_2 desorbed at 1200 s. (e) Cyclic capacity. (f) Relative heat duty.

Figure S7. Comparison of cyclic capacity for the different alcohol-MEA systems at different regeneration time. (a) cyclic capacity of MeOH-MEA system. (b) cyclic capacity of EtOH-MEA system.

Figure S8. Comparison of relative heat duty for methanol and ethanol addition system at 1200 s.

Figure S9. Influence of catalyst and ethanol solvent on CO_2 absorption performance.

Table S1. A brief review of research works for solvent regeneration process with different catalysts in the rich amine solvent.

Section S1. Materials

Monoethanolamine (99%), 2-(Methylamino)ethanol(99%), 2-(Ethylamino)ethanol (99%), 2-(Diethylamino)ethanol (99%), N,N-dimethylethanolamine (98%) and N-Methyldiethanolamine (99%), Amberlyst-15 resin, and Amberlite IR-120 resin were obtained from Shanghai Aladdin Industrial Corporation, China. Amberlite-732 resin, and Amberlyst-35 resin were purchased from Shanghai Macklin Chemical Reagent Co. Ltd., China. HCl (AR, 36.0 - 38.0%), methanol (AR, 99%) and ethanol (AR, 99%) were obtained from Sinopharm Chemical Reagent Co. Ltd., China. CO_2 (99.9%), and N_2 (99.99%) were acquired from Changsha Rizhen Gas Co. Ltd., China.

Section S2. Resin activation.

The different types of commercial ion exchange resins were activated by the impregnation method at room temperature in 2 M HCl for 24 h. After that, the ion exchange resins were washed with deionized water until the filtrate was neutral. Then, the ion exchange resins were washed with ethanol and dried at 60 °C for 24 h to give the final, activated catalysts used for this study.

Section S3. Catalyst characterization

Section S3.1. Nitrogen physisorption

The N_2 physisorption technique was used to measure the surface area, pore volume and pore size of the catalysts and was performed on the NOVA 2000e nitrogen adsorption desorption instrument. Before each analysis, the prepared catalyst sample was degassed at 120 °C for 8 h using helium. The pore volume and size were obtained by using the Barrett-Joyner-Halenda (BJH) method. The specific surface area was calculated by the Brunauer-Emmett-Teller (BET) theory.

Section S3.2. Total acid sites analysis

The Bronsted acid sites of the catalyst samples were measured by acid-base titration method as reported by Bozkurt et al [1]. Approximately 0.1 g catalyst was put into 20 mL of 2.0 M NaCl solution for 24 h. Then, the liquid was titrated with 0.01 M NaOH. The acid sites (mmol H^+/g_{cat}) were calculated in Eq S1 as follows:

$$The\ acid\ capacity = \frac{molarity\ of\ NaOH\left(\frac{mmol}{mL}\right) * volume\ of\ NaOH\ spent(mL)}{catalyst(g)} \tag{S1}$$

Section S4. Experimental apparatus

The experimental apparatus for CO_2 desorption and absorption mainly consisted of a round bottom four-neck flask as the batch reactor, a mass flowmeter (Beijing Seven-star Electronics Co., Ltd, China), a heating mantle (Henan Shengbo instrument Co. Ltd., China), an infrared CO_2 analyzer (GS10, Ennix, Germany), and an electricity meter (Zhejiang Tepsung electric Co.Ltd.) as presented in Figure S1.

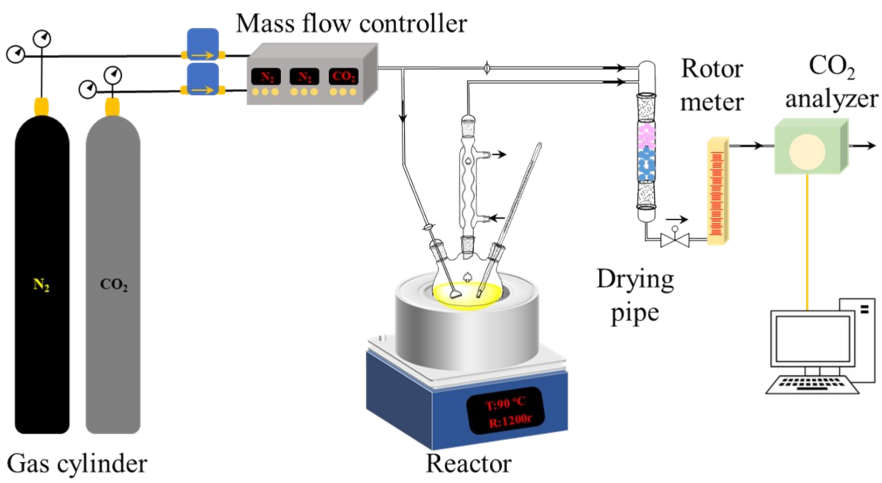

Figure S1. Schematic diagram of the experimental apparatus for CO_2 desorption and absorption.

Briefly, in the CO_2 desorption experiment, 500 mL (in sections 3.2.1, 3.2.2, 3.2.3) or 300 mL (in sections 3.2.4, 3.2.5, 3.4) CO_2-rich amine solution with or without catalysts or ethanol solvent were added into the round bottom flask. The desorption temperature was raised from 25 to 90 °C and held at 90 ± 0.1 °C. Also, the solution was stirred at 1200 rpm. The CO_2 released from the rich amine solution was cooled, dried, and mixed with 1 L/min N_2 carrier. Meanwhile, the CO_2 concentration was measured every ten seconds by an infrared CO_2 analyzer during the desorption experiment. The end of each desorption test was realized as the point where the concentration of CO_2 in the carrier gas was lower than 0.2%. The heat input for each desorption test was recorded by an electricity meter. However, this obtained value of the heat duty is higher than the actual value due to the simplified apparatus so that for this work the relative heat duty was used to compare the desorption performance.

For the CO_2 absorption experiment, a magnetic stirring rate of 1200 rpm with temperature set at 40 °C was used. The simulated flue gas (15 vol% CO_2, and 85 vol% N_2) with a total flowrate of 0.5 L/min was bubbled into the lean amine solution. The CO_2 concentration in the outlet gas was also recorded by an infrared CO_2 analyzer as aforementioned.

During the absorption and desorption processes, the amount of CO_2 absorbed or desorbed was determined by two quantitative methods. The gas phase measurement was obtained by the infrared CO_2 analyzer. The liquid phase measurement was made with Chittick apparatus [2]. The mass balance was verified by comparing the results from these two methods, and the average absolute relative deviations between gas and liquid phase measurements were within 5%.

Section S5. Analysis

The CO_2 reaction rate (r, mol/(s*L)) was measured through the CO_2 concentration by the infrared CO_2 analyzer in Eq S2, and the quantity of CO_2 desorbed ($N_{CO_2,gas}$, mmol) from the gas method was calculated in Eq S3 as follows:

$$r = \left|\frac{1}{22.4 \times V}\left(v_{CO_2}^{in} - \frac{X_{CO_2}^{out}}{1 - X_{CO_2}^{out}} \times v_{N_2}^{in}\right)\right| \tag{S2}$$

$$N_{CO_2,gas} = V\int_0^t r dt \tag{S3}$$

Here, V (L) represents the volume of amine solution, $v_{CO_2}^{in}$, $v_{N_2}^{in}$ (mol/s) represent the gas flowrates of CO_2 and N_2 from the mass flowmeter, respectively, and $X_{CO_2}^{out}$ (%) represents the CO_2 concentration of the outlet gas.

The quantity of CO_2 desorbed ($N_{CO_2,liquid}$, mmol) from the liquid method was calculated with Eq S4, and the cyclic capacity (mol/mol) was defined in Eq S5 as follows.

$$N_{CO_2,liquid} = (\alpha_{rich} - \alpha_{lean}) \times C \times V \tag{S4}$$

$$The\ cyclic\ capacity = \alpha_{rich} - \alpha_{lean} \tag{S5}$$

Here, α_{rich}, α_{lean} (mol CO_2/mol amine) represent the CO_2 loadings of rich and lean amine solution, respectively. C (mol/L) represents the concentration of the amine.

The heat duty (*HD*, kJ/mol) of amine regeneration was obtained from Eq S6, and the relative heat duty (*RHD*, %) was defined in Eq S7 for a fair comparison as follows.

$$HD = \frac{E_{electricity}}{N_{CO_2,gas}} \tag{S6}$$

$$RHD = \frac{HD_i}{HD_{baseline}} \times 100\% \tag{S7}$$

Here, $E_{electricity}$ (kJ) represents the energy consumption for amine regeneration recorded by the electricity meter, HD_i (kJ) represents the *HD* of different amine systems with catalysts or ethanol solvent, and $HD_{baseline}$ (kJ) represents the *HD* of the amine regeneration blank run.

Section S6. Influence of catalyst types at 80°C

To obtain a more convective conclusion on the catalyst performance for solvent regeneration, the catalytic activities of the studied catalysts were investigated at additional temperature of 80 °C, which is lower than the typical catalytic solvent regeneration temperature of 90 °C. As a result, the CO_2 desorption rates of CO_2-rich MEA solution with and without cation exchange resin catalysts at 80 °C are displayed in Figure S2. The peak CO_2 desorption rate of CO_2-rich MEA solution without catalyst was 4.614×10^{-5} mol/(s*L) at 1260 s. The maximum desorption rate of Amberlite IR-120 catalyst was 4.963×10^{-5} mol/(s*L) at 1260 s. This showed a slight improvement compared with the blank run. The Amberlyst-35 slightly improved the CO_2 desorption rate and achieved its maximum of 5.266×10^{-5} mol/(s*L) at 1180 s. Moreover, the peak desorption rate of CO_2-rich solution with Amberlite-732 and Amberlyst-15 catalysts were 5.566×10^{-5} and 5.571×10^{-5} mol/(s*L) at 1250 and 1200 s, respectively. It can be concluded that all the catalysts reached the maximum desorption rate earlier than the blank run, and the value of the peak CO_2 desorption rate was higher than for the MEA solution without catalysts. Moreover, the Amberlyst-15 catalyst best accelerated the proton transfer and best enhanced the CO_2 desorption rate.

In addition to the CO_2 desorption rate, the CO_2 desorption amount is improved in the first 1200 s at 80 °C. Only 12.0 mmol CO_2 was desorbed from CO_2-rich MEA solution without catalyst, while 13.8 mmol CO_2 was released when the Amberlite IR-120 was used. The Amberlyst-35 slightly enhanced the CO_2 desorbed amount to 14.5 mmol, and the quantities of CO_2 desorption attributed to the use of Amberlite-732 was 15.0 mmol. The best performance was exhibited by Amberlyst-15, which led to a CO_2 desorption amount of 16.3 mmol, 36% higher than that for CO_2-rich MEA solution without catalyst. Therefore, all the ion-exchange resin catalysts are capable of desorbing greater amounts of CO_2 compared to the blank run, thus reducing the heat duty of MEA solution regeneration because the heat duty is related to the quantity of CO_2 desorbed per unit of energy consumption. The Dowex D001, Amberlite IR-120, and Amberlyst-35 slightly reduced the heat duty by around 7.7, 12.7, and 17.2% compared with the noncatalytic MEA solution system, respectively. Also, the Amberlite-732 decreased the heat duty by around 20.0%. It is noteworthy that the Amberlyst-15 catalyst minimized the heat duty up to 26.2%, demonstrating its superior

MEA regeneration efficiency. In terms of the relative heat duty, the catalytic performance trend was seen to be Amberlyst-15 > Amberlite-732 > Amberlyst-35 > Amberlite IR-120 > Dowex D001 > no catalyst, which is consistent with the trend measured at 90°C.

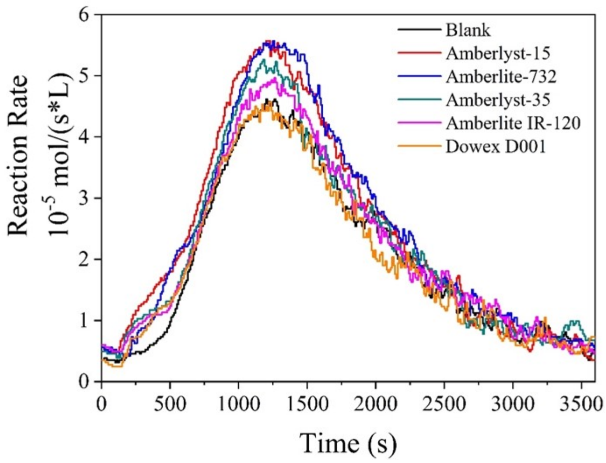

Figure S2. The CO_2 desorption rate curves with different catalysts at 80 °C.

Section S7. Influence of initial CO_2 loading

According to the VLE model of the MEA-CO_2-H_2O system, the mole fraction of HCO_3^- increases with increasing CO_2 loading, while the mole fraction of CO_3^{2-} is negligible. Figure S2a presents the desorption rate curves for catalytic and noncatalytic MEA systems with initial CO_2 loading of 0.53, 0.51, and 0.49 mol CO_2/mol MEA. The amount of CO_2 desorbed in 1200 s with and without catalyst is compared in Figure S2b. As can be seen, with a decrease in initial CO_2 loading, the quantities of CO_2 desorbed within 1200 s tended to decrease linearly. As shown in Figure S2b, the MEA blank run could desorb 92.00, 57.00, 35.00 mmol CO_2 with the initial CO_2 loading of 0.53, 0.51, and 0.49 mol CO_2/mol MEA, respectively. The Amberlyst-15 catalyst with CO_2 initial loading of 0.53 and 0.51 mol CO_2/mol MEA increased the quantities of CO_2 released by 21.47%, 26.75%. The highest increment by 39.29% in the desorbed amount of CO_2 was presented for the initial CO_2 loading of 0.49 mol CO_2/mol MEA with 2 wt.% Amberlyst-15.

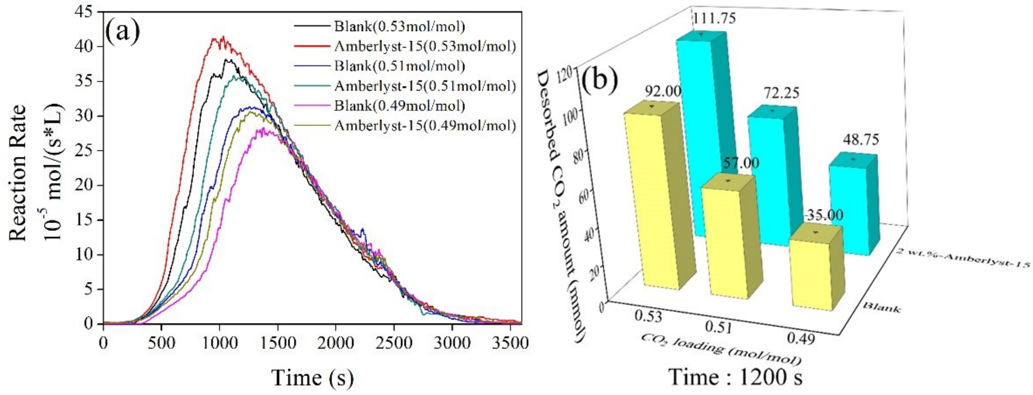

Figure S3. The CO_2 desorption performance with different initial CO_2 loading. (a) CO_2 desorption rate curves. (b) Total amount of CO_2 desorbed at 1200 s.

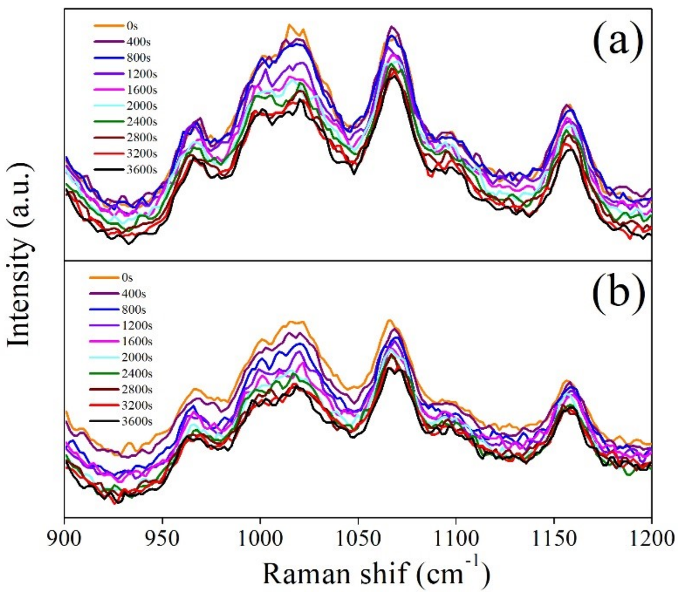

Figure S4. Raman spectra of MEA solution at various periods. (a) CO_2 desorption without catalyst. (b) CO_2 desorption with 2 wt.% Amberlyst-15.

Section S8. Influence of catalyst/MEA solvent ratio

As aforementioned, the Amberlyst-15 exhibited superior catalytic performance among the ion exchange resin catalysts. Of interest then, is the influence of catalyst/MEA solvent ratio on CO_2 desorption performance. To study this, the amounts of 1, 2, and 3 wt.% of catalyst were introduced into CO_2-rich MEA solutions, and the desorption rate, the amount of CO_2 released, and the relative heat duty were compared and illustrated in Figure S4a-S4b. From Figure S4a, it is clear that an insignificant improvement was observed in the desorption rate with the catalyst/MEA solvent ratio of 1 wt.%. With the catalyst/MEA solvent ratio at 2 wt.% and at 3 wt.% there was obvious but similar enhancement of the desorption rate. As shown in Figure S4b, when the catalyst/MEA solvent ratio was increased from 1 wt.% to 2 wt.%, the amount of CO_2 released increased, which could be attributed to the increase in the number of catalyst proton acid sites in the system. But when the catalyst/MEA solvent ratio was further increased up to 3 wt.%, the amount of CO_2 desorbed only increased slightly, which may be due to excess catalyst leading to transfer resistance.

The regeneration heat duty with different ratios is also presented in Figure S4b, and the 2 wt.% Amberlyst-15 showed lower relative heat duty of 78.89% than that of 1 wt.% Amberlyst-15 of 93.06%. While the 3 wt.% Amberlyst-15 presented the lowest heat duty of 75.75%, this is only slightly lower than for the 2 wt.%. Hence, the optimal ratio of catalyst/MEA solvent is 2 wt.% in this study, which is consistent with the results by Zhang et al [3].

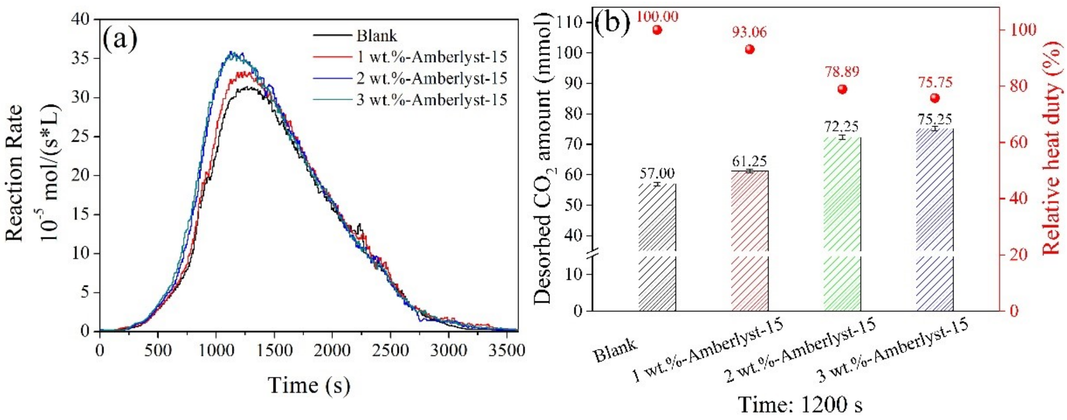

Figure S5. The CO_2 desorption performance with different catalyst/MEA solvent ratios. (a) CO_2 desorption rate curves. (b) Total amount of CO_2 desorbed and relative heat duty at 1200 s.

Section S9. Influence of methanol concentration

Figure S5a shows the desorption rate of 5 M MEA with different methanol concentrations, and it is clear that the methanol solvent significantly enhanced the desorption kinetics. In the MEA-water blank test run, the maximum CO_2 desorption rate only reached 2.613×10^{-4} mol/(s*L) at 1120 s. Under the same condition, methanol-MEA-water blend solvent with 5, 10, 12.5, 15 wt.% methanol reached maximal release rate of CO_2 of 3.803×10^{-4} mol/(s*L), 5.097×10^{-4}mol/(s*L), 5.748×10^{-4}mol/(s*L) and 6.252×10^{-4}mol/(s*L), at 1130 s, 1010 s, 1100 s and 1050 s, respectively. In comparison with the blank MEA solvent, the maximum value of CO_2 desorption rate was notably improved with the increasing of methanol concentration. However, above the methanol concentration of 20 wt.%, only a slight improvement was observed in the maximum desorption rate in comparison with the concentration of 15 wt.% at 6.252×10^{-4}mol/(s*L). Considering that too high a methanol concentration may cause a large amount of volatilization in the absorption process, the optimal methanol concentration is 15 wt.%.

The different quantities of CO_2 released over 1200 s is given in Figure S5c- S5d. The blended solvent with various concentrations of methanol not only improved the release kinetics but also increased the amount of CO_2 desorbed. As illustrated in Figure S5d, only 42.45 mmol CO_2 is released from the blank 300 mL of 5 M CO_2-rich MEA in 1200 s, while the rapid kinetics of the methanol/MEA/water solvent resulted in 58.95 to 116.40 mmol CO_2 with methanol concentration in the range of 5-20 wt.%. In comparison with the 15 wt.% methanol solvent, insignificant improvement in CO_2 desorption quantity was presented with the higher 5 wt.% methanol solvent addition, namely, 20 wt.%.

To further investigate the effect of methanol concentration on CO_2 desorption, the CO_2 loading curves as a function of time and the cyclic capacity are compared in Figure S5b and Figure S5e, respectively. Figure S5b summarizes the CO_2 loading over 3600 s of desorption process. The CO_2 loading at the end of the desorption step is 0.44 mol CO_2/ mol MEA for the blank MEA solvent, which shows a poor cyclic capacity of 0.07 mol CO_2/ mol MEA at the low temperature of 90 °C. However, methanol/MEA/water solvent presents an excellent regeneration ability and cyclic capacity under the same temperature. Among the different concentrations of methanol, the 20 wt.% methanol-MEA-water solvent shows a cyclic capacity as high as 0.26 mol CO_2/ mol MEA, an improvement of 3.7 times compared with that of blank MEA solvent. It should be noted that the cyclic capacity is already about 0.23 mol CO_2/ mol MEA achieved with the concentration of methanol at 15 wt.%, only slightly less than the 20 wt.% methanol solvent. Overall, these results demonstrate that the addition of methanol could significantly enhance the cyclic capacity of MEA based solvent. In addition to improving the cyclic capacity to achieve practical industrial requirements at low temperature, the regeneration heat duty was also reduced because greater quantities of CO_2 were released with the same reaction time.

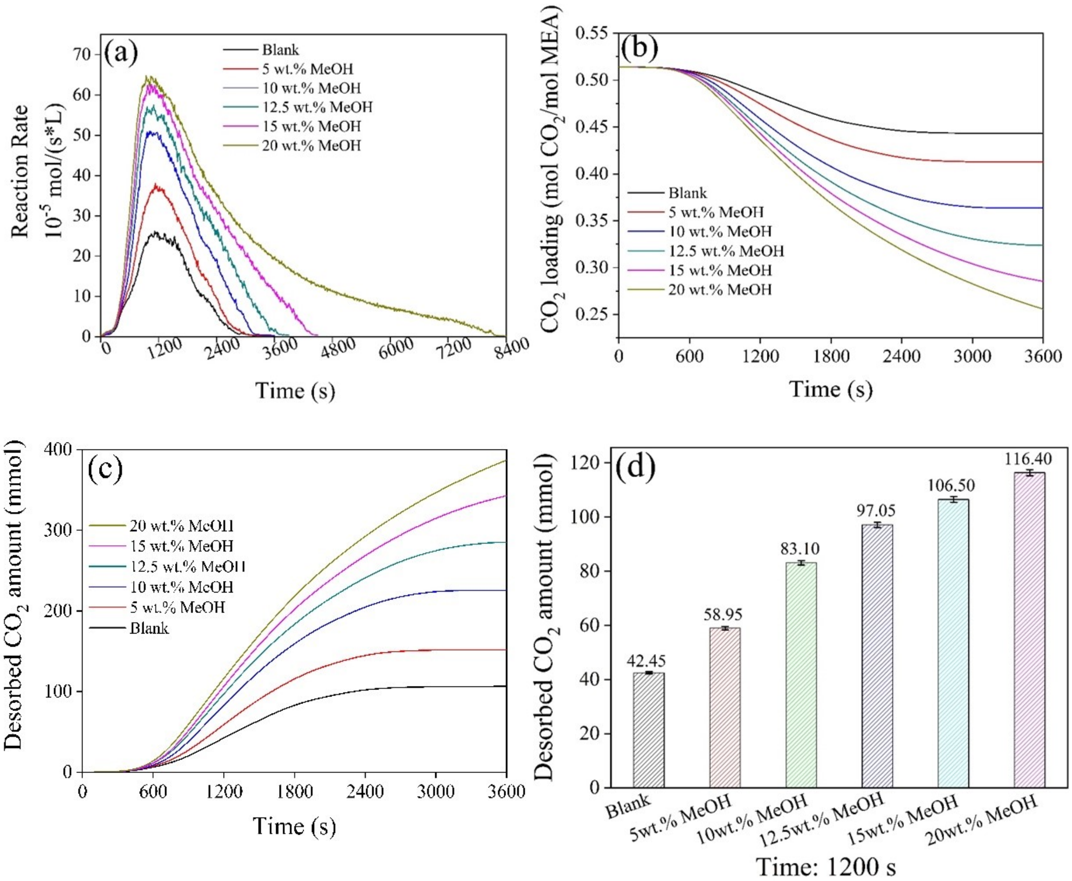

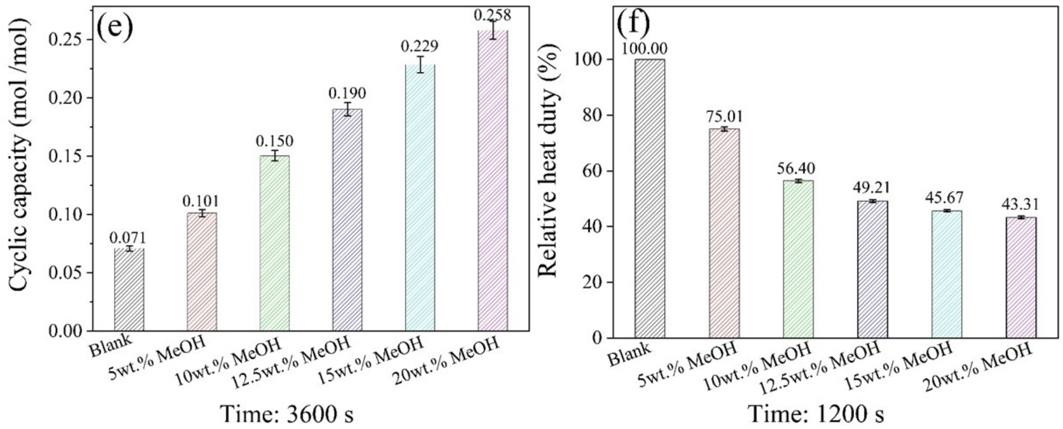

Figure S6. Effect of methanol concentration on CO_2 desorption performance at 90 °C. (a) CO_2 desorption rate curves. (b) CO_2 loading curves. (c) Desorbed CO_2 amount curves. (d) Total amount of CO_2 desorbed at 1200 s. (e) Cyclic capacity. (f) Relative heat duty.

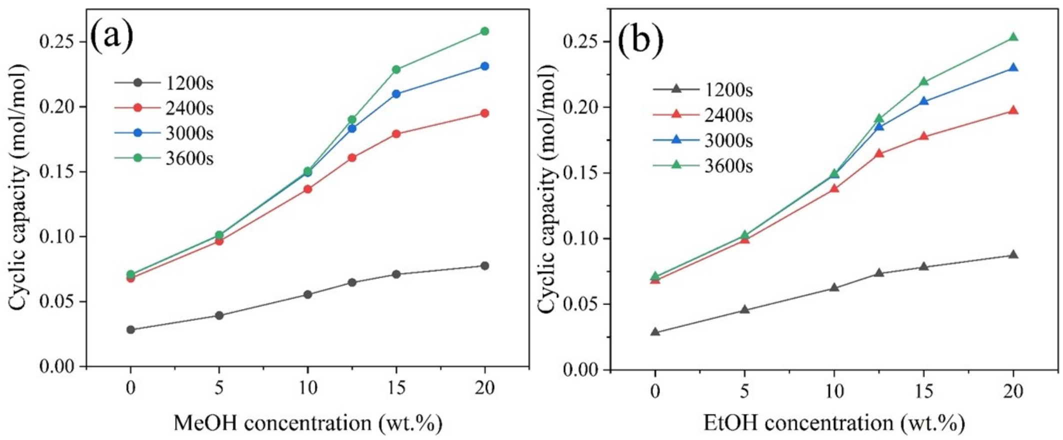

Figure S7. Comparison of cyclic capacity for the different alcohol-MEA systems at different regeneration time. (a) cyclic capacity of MeOH-MEA system. (b) cyclic capacity of EtOH-MEA system.

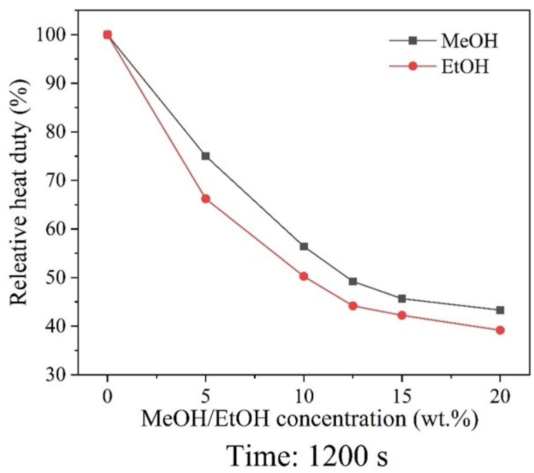

Figure S8. Comparison of relative heat duty for methanol and ethanol addition system at 1200 s.

Section S10. Effect of catalyst and ethanol on CO_2 absorption performance

Evaluating the CO_2 absorption process is an important part of understanding thermal amine-based CO_2 capture technology. Thus, examining the effect of Amberlyst-15 catalyst and ethanol solvent on CO_2 absorption performance is required. The CO_2 absorption curves of CO_2 loading as a function of time for blank, catalyst-MEA-water and catalyst-EtOH-MEA-water systems are presented in Figure S8. Note that there is no significant difference in catalyst-MEA-water and catalyst-EtOH-MEA-water systems compared with the blank run. Consequently, it can be concluded that the introduction of catalyst and ethanol solvent had no negative effect on the CO_2 absorption process in terms of CO_2 loading and absorption rate.

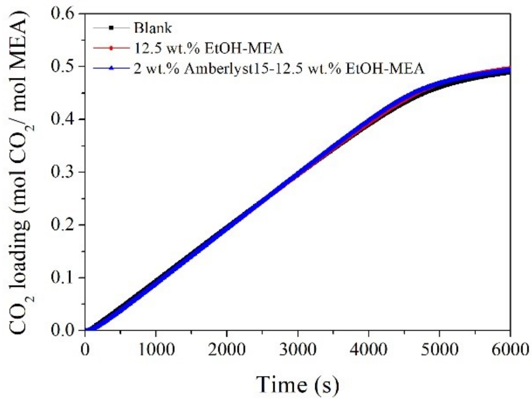

Figure S9. Influence of catalyst and ethanol solvent on CO_2 absorption performance.

Table S1. A brief review of research works for solvent regeneration process with different catalysts in the rich amine solvent.

Catalyst	Single/blend solvent	Desorption temperature (°C)	Main results	References
γ-Al_2O_3/HZSM-5, HZSM-5, HY, γ-Al_2O_3	MEA	50-105	Mixture catalysts presented better performance than single catalysts; Amount of desorbed CO_2 increased by 20.1-31.2%; Heat duty reduced by 16.9-23.7%.	(Liang et al., 2016)[4]
SAPO-34, SO_4^{2-}/TiO_2	MEA	70-96	SAPO-34 showed better performance than SO_4^{2-}/TiO_2; Amount of desorbed CO_2 increased by 14.1-28.2%; Heat duty reduced by 17.1-24.3%.	(Zhang et al., 2017)[5]
HZSM-5, MCM-41, SO_4^{2-}/ZrO_2	MEA	70-98	Performance, HZSM-5 > MCM-41 > SO_4^{2-}/ZrO_2; Amount of desorbed CO_2 increased by 10.6-29.4%; Heat duty reduced by 9.8-24.8%.	(Liu et al., 2017)[6]
Nanoparticles SiO_2, TiO_2, Al_2O_3	MEA	103	The TiO_2 shows best performance, and the use of TiO_2 nanoparticles saved desorption time by 42%.	(Wang et al., 2016)[7]
V_2O_5, MoO_3, WO_3, TiO_2, and Cr_2O_3,	MEA	35-86	Performance, MoO_3 > V_2O_5 > Cr_2O_3 > TiO_2 > WO_3; Amount of desorbed CO_2 increased by 44-	(Bhatti et al., 2017)[8]

			94%; Sensible heat reduced by 25-48%.	
SZMF	MEA	60-98	Amount of desorbed CO_2 increased by 38.1-54.7%; Heat duty reduced by 27.7-39.4%.	(Zhang et al., 2019)[9]
SO_4^{2-}/ZrO_2-HZSM-5	MEA	98	Amount and rate of CO_2 desorption increased by 40 and 37%; Energy consumption reduced by approximately 31%.	(Xing et al., 2020)[10]
SO_4^{2-}/ZIF-67-C@TiO_2	MEA	88	Amount and rate of CO_2 desorption increased by 64.5 and 153%; Energy consumption reduced by approximately 36%.	(Xing et al., 2021)[11]
γ-Al_2O_3/HZSM-5, HZSM-5, γ-Al_2O_3	MEA-BEA-AMP	90	The combination of "tri-solvent + heterogeneous catalysts" was 0.3+2+2 mol/L MEA+BEA+AMP + blended γ-Al_2O_3/H-ZSM-5 = 2:1, whose relative heat duty (%) was 32.9% compared to 5.0 M MEA as a benchmark.	(Shi et al., 2021)[12]
V_2O_5, WO_3, and TiO_2,	DGA-DEGMME	90	V_2O_5, WO_3, and TiO_2 were found to be effective in decreasing the relative heat duty by 23.5%, 14.6%, and 14.4%, respectively.	(Bhatti et al., 2021)[13]
Fe/Ni@COF	MEA	88	The obtained nanomaterials achieve a considerable improvement in CO_2 desorption amount, representing a substantial increase of 540% relative to traditional thermal desorption.	(Li et al., 2022)[14]
CeO_2-MOF-HPW	MEA	88	The CO_2 desorption capacity and rate were increased by 38.1% and 166%, respectively, and the desorption energy consumption was reduced by 29.4% in comparison with the un-catalytic process.	(Wei et al., 2022)[15]

References

1. O. D. Bozkurt, N. Baglar, S. Celebi and A. Uzun, *Catal. Today*, 2020, **357**, 483-494.
2. W. J. G. B. C. Horwitz, Menasha, WI, 1975.
3. J. Zhang, D. Fu and J. Wu, *Journal of Environmental Sciences*, 2012, **24**, 743-749.
4. Z. Liang, R. Idem, P. Tontiwachwuthikul, F. Yu, H. Liu and W. Rongwong, *AlChE J.*, 2016, **62**, 753-765.
5. X. Zhang, X. Zhang, H. Liu, W. Li, M. Xiao, H. Gao and Z. Liang, *Applied Energy*, 2017, **202**, 673-684.
6. H. Liu, X. Zhang, H. Gao, Z. Liang, R. Idem and P. Tontiwachwuthikul, *Industrial & Engineering Chemistry Research*, 2017, **56**, 7656-7664.
7. T. Wang, W. Yu, F. Liu, M. Fang, M. Farooq and Z. Luo, *Industrial & Engineering Chemistry Research*, 2016, **55**, 7830-7838.
8. U. H. Bhatti, A. K. Shah, J. N. Kim, J. K. You, S. H. Choi, D. H. Lim, S. Nam, Y. H. Park and I. H. Baek, *ACS Sustainable Chemistry & Engineering*, 2017, **5**, 5862-5868.
9. X. Zhang, Z. Zhu, X. Sun, J. Yang, H. Gao, Y. Huang, X. Luo, Z. Liang and P. Tontiwachwuthikul, *Environmental science & technology*, 2019, **53**, 6094-6102.
10. L. Xing, K. X. Wei, Q. W. Li, R. J. Wang, S. H. Zhang and L. D. Wang, *Environmental Science & Technology*, 2020, **54**, 13944-13952.
11. L. Xing, K. Wei, Y. Li, Z. Fang, Q. Li, T. Qi, S. An, S. Zhang and L. Wang, *Environmental Science & Technology*, 2021, **55**, 11216-11224.
12. H. Shi, X. Yang, H. Feng, J. Fu, T. Zou, J. Yao, Z. Wang, L. Jiang and P. Tontiwachwuthikul, *Industrial & Engineering Chemistry Research*, 2021, **60**, 7352-7366.
13. U. H. Bhatti, A. Ienco, M. Peruzzini and F. Barzagli, *Acs Sustainable Chemistry & Engineering*, 2021, **9**, 15419-15426.
14. Y. Li, Z. Chen, G. Zhan, B. Yuan, L. Wang and J. Li, *Sep. Purif. Technol.*, 2022, **298**, 121676.
15. K. X. Wei, L. Xing, Y. C. Li, T. Xu, Q. W. Li and L. D. Wang, *Sep. Purif. Technol.*, 2022, **293**.